Chapter:5

ESR performance of synthesized Ni/Co_3O_4-$LaCoO_3$ from deactivated Co-catalyst

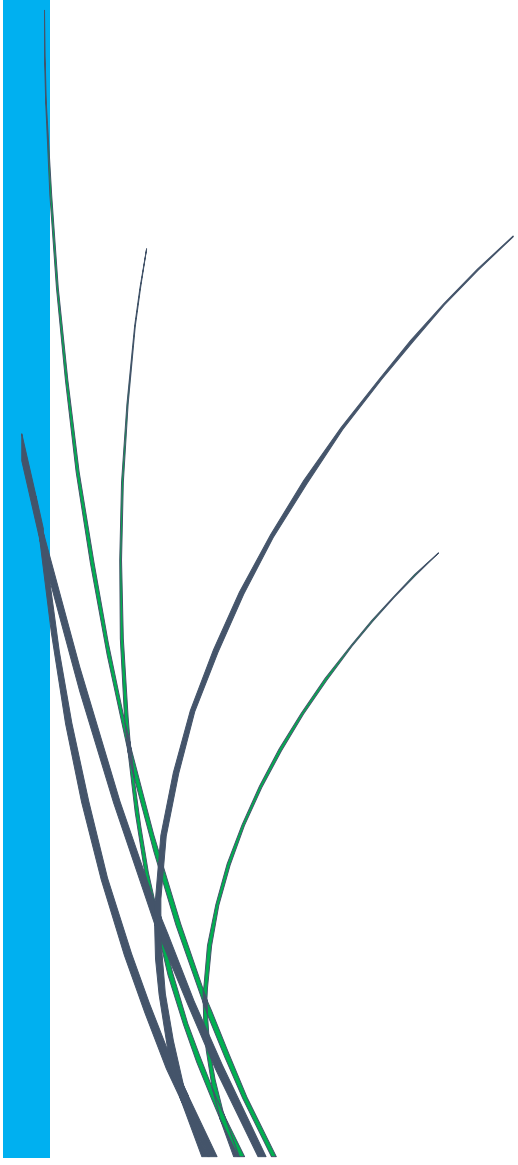

5.1 Introduction

The catalyst cost increases by using noble metals. However, noble metal catalysts are typically highly stable, but carbon deposition has also been reported to decrease catalytic activity [18, 26, 32]. The high cost of catalyst affects the overall cost of renewable hydrogen generation [268]. Hence, the catalyst regeneration or catalyst reformulation from deactivated catalyst can be a cost effective approach. If high temperature tolerant catalyst can be synthesized, then after carbon deposition it can be regenerated by oxidation of carbon at optimum temperature. The special structured mixed metal oxide such as spinel, perovskite and hydrotalcite have homogenous distribution of atoms as well as excellent sintering stability.

Literature survey suggests that most of the ESR were carried out with La_2O_3 as a support, mixed oxide or as a promoter with other supports [88, 269-277]. Perovskite catalysts have typically low surface area but several advantages comparable to noble metal catalysts [278]. The general formula, ABO_3 of perovskite has the possibility of partial substitution or a complete substitution at A as well as at B sites with number of elements. The A site must contains larger size cation as compared to that B site [279]. The textural structure of $LaCoO_3$ affects its catalytic properties, which is directly correlated with the method of preparation [280, 281]. Nonetheless, the ESR study were reported with $LaNiO_3$, and with partial substitution at B sites with Co and Ni as $LaCo_xNi_{1-x}O_3$ and $LaNi_xCo_{1-x}O_3$ [47, 103, 119, 158].

Among non-noble metal catalyst, Ni and Co have shown viable catalytic performance regarding hydrogen selectivity [68, 90, 126, 152, 222, 244, 253, 256, 258-260, 282-289]. In metallic state Co is not only active to perform the ESR but also facilitates the filamentous carbon formation and get deactivated [151, 252, 290-295]. However, this deactivated form of cobalt-carbon contains highly dispersed Co metal.

Therefore, considering these prospects, this work has been intended to reutilize this deactivated catalyst for perovskite-cobalt composite catalyst preparation. In the nanocasting methods, profoundly silica (KIT 6, MCM 48 and SBA 15) or carbon based templates are used [296, 297]. The catalyst to be used in thermally treated reactions must be temperature tolerant. In the nanocasting method, the removal of template can be chemical or thermal. The catalyst prepared through thermal leaching of templates is more appropriate to be used in high temperature reactions. In this work Co and carbon nanofilament formed during ESR over Co metal is used for $LaCoO_3$-Co_3O_4 catalyst synthesis. The $LaCoO_3$ based composite preparation has been selected, because perovskite structure formation requires high-temperature calcination and similarly the elimination of carbon templates. However, there is a chance of Co_3O_4 sintering due to high temperature calcination. Hence, the activity might be reduced but the bimetallic interaction may facilitate the hydrogen generation [298]. The composite was further impregnated with Co and Ni to check how the active metals interaction with composite affects their performance for renewable hydrogen generation via ESR, because bimetallic interactions have shown positive effect on conversion and selectivity of produced gases [299]. The study of the perovskite-cobalt composite as a support was still unrevealed with ESR. Therefore, this study enlightens the role of the Co_3O_4-$LaCoO_3$ composite and its interaction with Ni and innovative catalyst formulation by waste or catalyst regeneration via nano-casting approach for renewable hydrogen generation.

5.2 Experimental

5.2.1. Catalyst preparation

Three types of catalyst viz. Co_3O_4-$LaCoO_3$, 10%Ni/Co_3O_4-$LaCoO_3$ and 10%Co/Co_3O_4-$LaCoO_3$ were prepared. First of all the Co_3O_4-$LaCoO_3$ was prepared following the nano-casting approach, here spent catalyst containing nano-filamentous

carbon formed on Co was taken for the synthesis of catalyst. The Co with carbon template was obtained by performing ESR over barren metallic Co (produced by *in-situ* thermal decomposition of $CoC_2O_4.2H_2O$ in the inert atmosphere) catalyst as described in Chapter-4. The Co and C template in water was sonicated for 15 min with the help of ultra-sonication bath to disperse them homogeneously in water. The solution of $La(NO_3)_2.6H_2O$ and citric acid was prepared in ethanol with desired concentration (Molar ratio of metal ions to citric acid = 2:1). It was added in the above Co with C template dispersed in water and stirred overnight at room temperature. Now, it was heated with stirring at 373K until a gel-like appearance was visible. After drying overnight, it was calcined in two steps, flowing air (30ml/min) at 773K for 4h and 973K for 6h to burn the filamentous carbon and formation of composite Co_3O_4-$LaCoO_3$. The prepared Co_3O_4-$LaCoO_3$ was used as a support for the preparation of 10%Ni/Co_3O_4-$LaCoO_3$ and 10%Co/Co_3O_4-$LaCoO_3$ by wet impregnation method using $Ni(NO_3)_2.6H_2O$ and $Co(NO_3)_2.6H_2O$ as metal precursors. Ethanol was used as impregnation medium for each catalyst with vigorous stirring for 5h at room temperature. Then after, the stirring was done at 333K until appearance of fuzziness in mixture and then it was kept in oven at 373K overnight. After drying each precursor, calcination was done at 873K for 2h to obtain the catalysts.

5.2.2 ESR Performance test

To find out the activity of prepared catalyst, ESR were performed within the temperature range of 573K-873K at the interval of 50K. Before the ESR performance both of the catalyst were reduced at 773K for 3h by flowing H_2 (99.999% purity, rate =10ml/min) environment. After reduction, reactor was flushed with Ar (99.999%) to provide the inert environment in a fixed bed tubular quartz reactor with inner diameter 0.9cm and length of 40cm. The quartz wool was used to prepare the bed of the catalyst

by taking 100mg of catalyst. The reactant mixture was fed at a constant rate (4ml/h) into the designed quartz preheater through a syringe pump. The temperature of the preheater was kept constant at 473K.

5.3 Results and discussion

5.3.1 Characterization studies

5.3.1.1 Textural properties

The surface area of Co-C filament prepared has high surface area and pore volume, compared to the above synthesized perovskite based catalysts (table 5.1). The perovskite preparation includes high temperature to form its structure and at that temperature sintering of catalyst occurred. It may be the reason for reduction of surface area. After impregnation, the surface area of catalysts were still comparable to each other.

Table 5.1 Surface area and pore volume of different catalyst and Co-C filament.

Catalyst	Surface area (m^2/g)	Pore Volume(ml/g)
Co-C (spent)	108.2	0.160
Co_3O_4-$LaCoO_3$	2.7	0.004
Ni/Co_3O_4-$LaCoO_3$	2.7	0.003
Co/Co_3O_4-$LaCoO_3$	2.7	0.003

5.3.1.2 XRD analysis

Figure 5.1 represents the HR-XRD of the Co-C nanofilament, prepared catalysts and rietveld refinement performed for Co_3O_4-$LaCoO_3$. The Co-C nano-filament graph shows intense peak at 2θ value 26° (JCPDS 75-1621) of graphitic carbon and Co metal peaks at 44.20°, 51.53° and 75.87° (JCPDS 89-4307). However, the peak of carbon was entirely absent in synthesized catalysts.

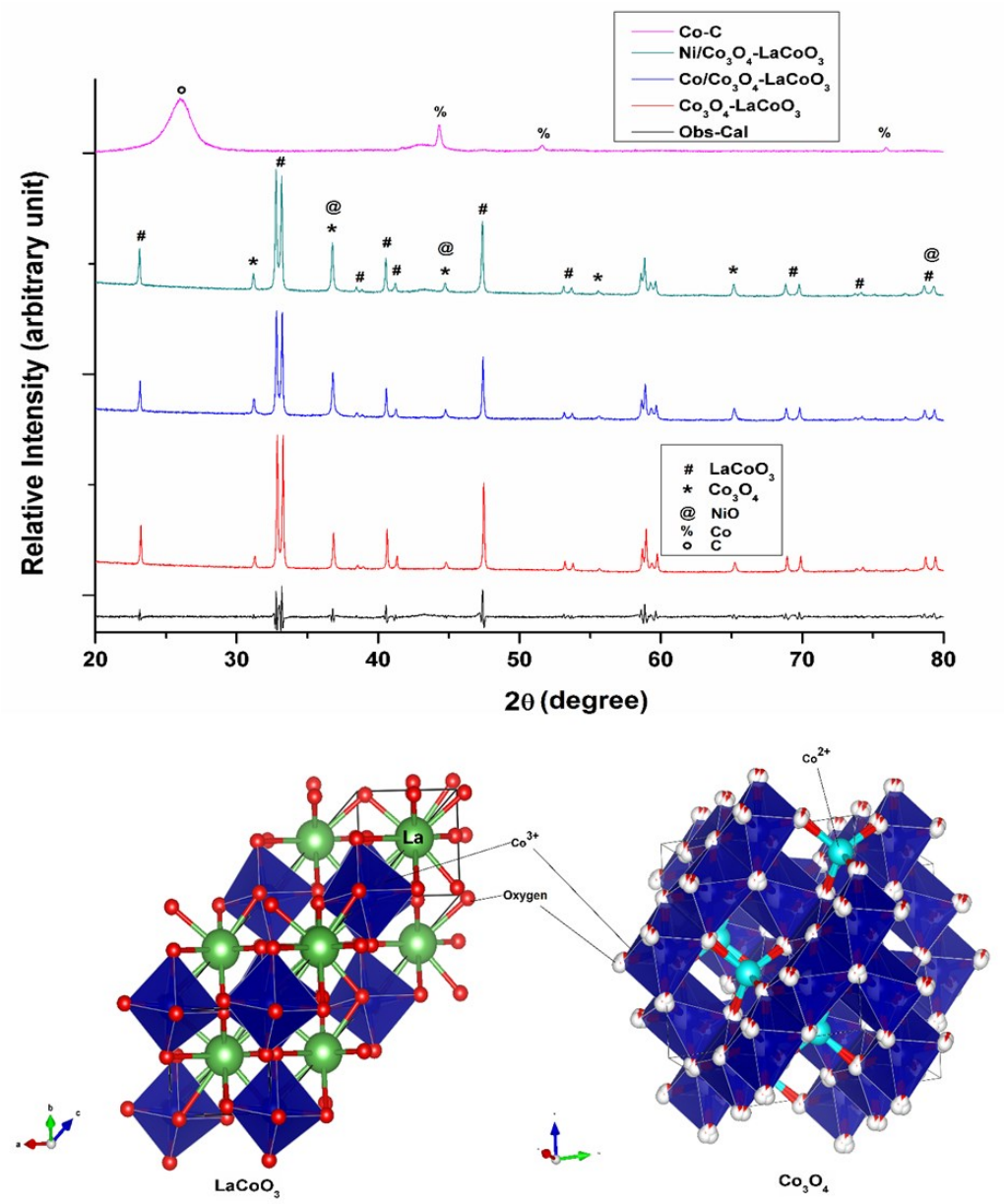

Figure 5.1 HR-XRD analysis of each catalyst and crystal structure obtained after rietveld refinement of Co_3O_4- $LaCoO_3$.

The intense peak of Co_3O_4 at 2θ, 36.85° with the plane (311) confirms its presence in Co_3O_4-$LaCoO_3$. However, the 2θ values 37.25° (111), 43.28° and 79.40° of NiO is in agreement with JCPDS-65-5745 but it also coincides with the 2θ value of Co_3O_4 and $LaCoO_3$. For the confirmation of metallic Co and NiO existence in the respective catalyst, XPS results were further analysed. The synthesized $LaCoO_3$ was also confirmed with JCPDS- 48-0123 with 2θ value 23.22°, 32.87°, 33.29°, 38.95°, 40.65°, 41.33°, 47.49°, 53.22°, 53.80°, 58.71°, 58.98°, 59.76°, 68.96°, 69.92°, 73.86°, 74.33°, 75.26°, 78.76°,

79.45°. The chi-square value obtained by a Rietveld refinement of Co_3O_4-$LaCoO_3$ data was 9.3. Hence, the mixed two-phase composite oxide of spinel (Co_3O_4) and perovskite ($LaCoO_3$) was confirmed. The catalyst structure drawn for Co_3O_4 and $LaCoO_3$ have shown cobalt (Co^{3+}) and lanthanum (La^{3+}) in the octahedral form (Figure 5.1). The Co_3O_4 also contains the tetrahedral form of cobalt (Co^{2+}).

5.3.1.3 Morphology analysis

Figure 5.2 represents the morphological analysis of catalyst and planner analysis by HR-TEM imaging techniques. Figures 5.2 (a) and (b) account for the TEM image of Co metal and Co-C nano-filament. The image of Co-C nano-filament mixture has shown abundant carbon nanotube with diameter range 50-80 nm. The effective ionic radii of La^{3+} ion is 0.12 nm, and therefore it can interchange to any region of carbon nano-filament during agitation. Hence, we prefer to do agitation for 24h during the preparation of the catalyst. The AFM, HR-SEM and TEM image analysis confirm the particle size in a range of 120-170nm. The height of particle from AFM image was found maximum up to 6.5nm. The crystal structure in the fused rhombohedral hexagonal structure with cubic forms can be considered from TEM image ($LaCoO_3$-Co_3O_4), which is in agreement of crystal structure obtained from Rietveld refinement. Moreover, the absence of any single carbon nano-filament in the TEM images are in agreement with HR-XRD data. The HR-SEM and TEM image both have shown regular distribution of active metals (Co and Ni) at the surface of $LaCoO_3$-Co_3O_4 composite after impregnation. The HR-TEM images have shown Co_3O_4 (311) and NiO (111) abundant planes as obtained by HR-XRD analysis. The planes of $LaCoO_3$-Co_3O_4 composite have not been marked because the value of d-spacing was found comparable to Co_3O_4 as well as for $LaCoO_3$.

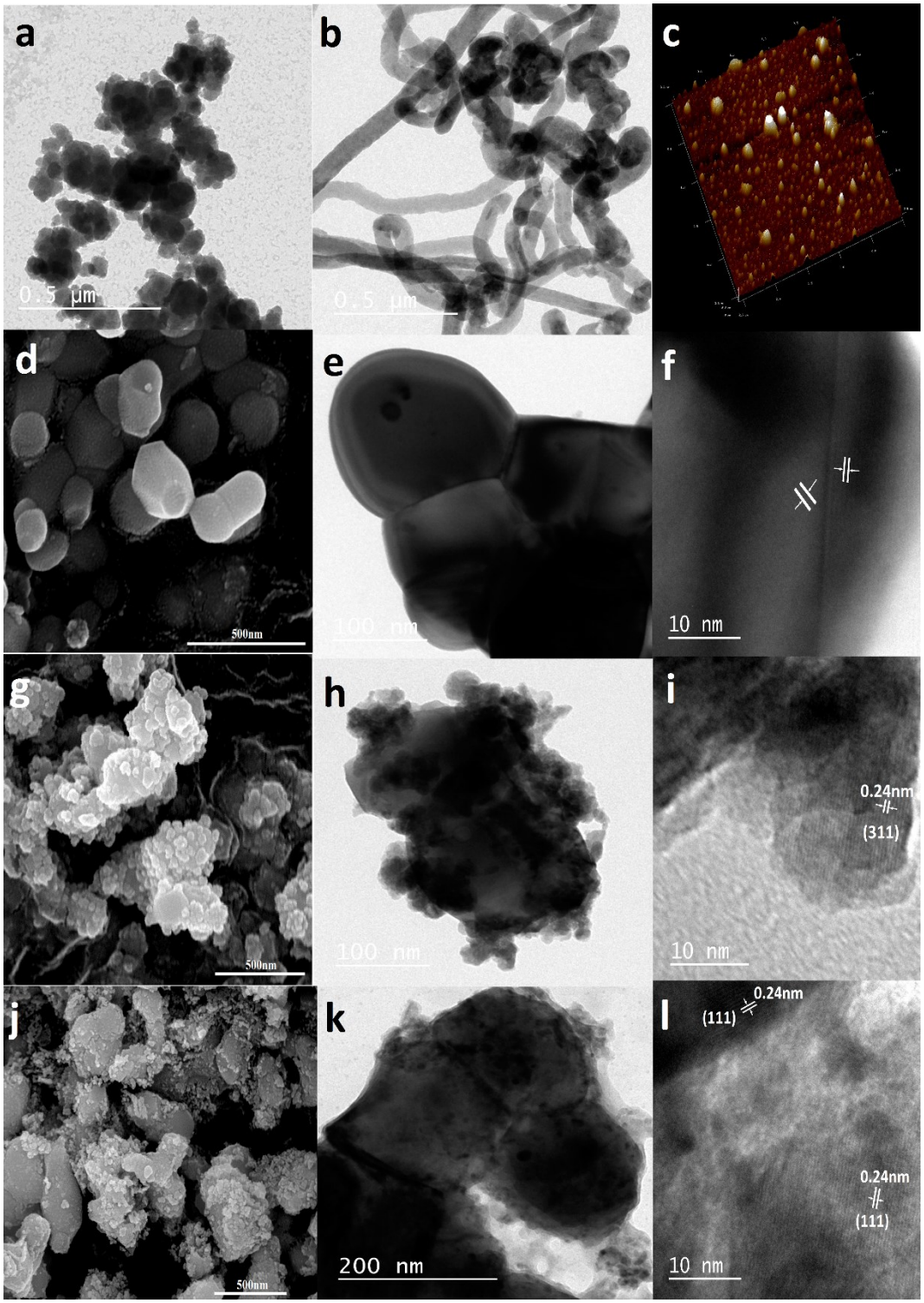

Figure 5.2 TEM images of Co (a), Co-C (b), Co_3O_4-$LaCoO_3$ (e), Co/Co_3O_4-$LaCoO_3$ (h) and Ni/ Co_3O_4-$LaCoO_3$ (k). AFM image of Co_3O_4-$LaCoO_3$ (c). HR-SEM and HR-TEM analysis of Co_3O_4-$LaCoO_3$ (d and f), Co/Co_3O_4-$LaCoO_3$ (g and i) and Ni/ Co_3O_4-$LaCoO_3$ (j and l) respectively.

5.3.1.4 TPR analysis

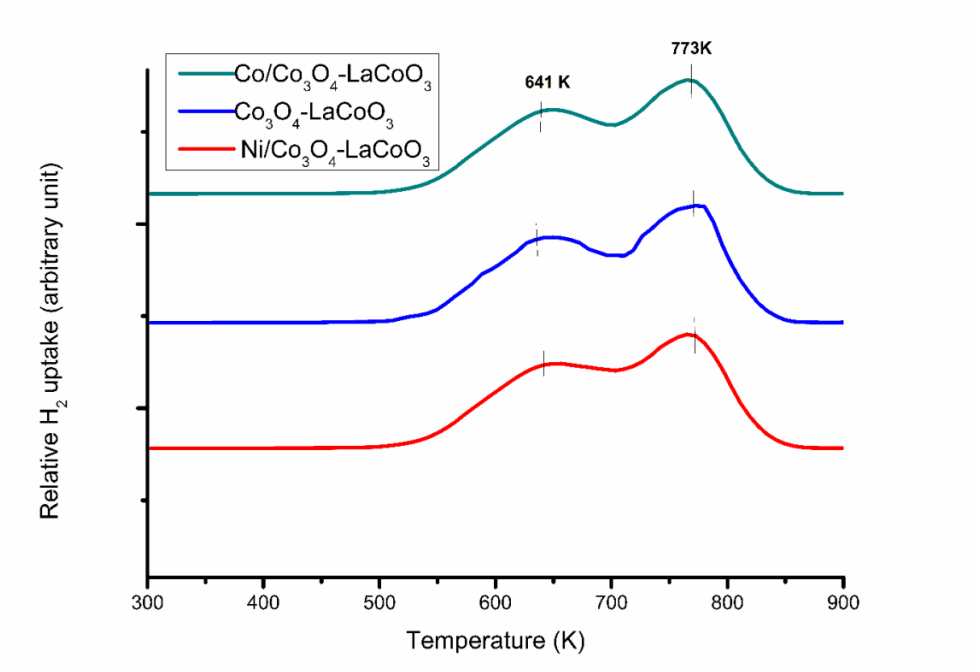

Figure 5.3 TPR profile of the Co/Co_3O_4-$LaCoO_3$, Co_3O_4-$LaCoO_3$ and Ni/Co_3O_4-$LaCoO_3$ catalysts.

The TPR graph (Figure 5.3) of prepared composite catalysts has shown two major peaks at 641K and 773K. These temperatures can be assigned for the two-step reduction of Co_3O_4. First step reduction of Co_2O_3 to CoO and the second one is from CoO to Co^0. All of the catalysts contain Co_3O_4 in equivalent concentration. The Co^{3+} to Co^0 is also possible for the Co species present in $LaCoO_3$ at 673K [300]. However, Ni/ Co_3O_4-$LaCoO_3$ contains NiO, which get reduced at temperature ≈ 700K. Hence, the peak of Ni comprises in that region for Ni/ Co_3O_4-$LaCoO_3$. The reduction temperature was lower as compared to the B sites substitution of perovskite as reported by Zhao et al. [300] and it is in agreement with the work reported by Simanote et al [301].

Figure 5.4 represents the XPS of Co, La, O and Ni in particular catalyst Co_3O_4-$LaCoO_3$, Co/Co_3O_4-$LaCoO_3$ and Ni/ Co_3O_4-$LaCoO_3$. The HR-XRD analysis of the synthesized catalyst has shown Co_3O_4 peaks. However, 2θ value with highest intensified peak of Co was found near to 44° might been overlapped with Co_3O_4. Therefore, XPS

were performed for the confirmation of different Co oxidation states. The peaks were deconvoluted typically for Co.

5.3.1.5 XPS analysis

The XPS spectra of Co_3O_4 was found complicated to deconvolute because of presence of variable oxidation states of Co in Co_3O_4 and $LaCoO_3$. The Co_3O_4 is a spinel which is composed of CoO and Co_2O_3. In the CoO, Co is in tetrahedral form, whereas in Co_2O_3, it is in octahedral form. The octahedral form of Co will also be present in $LaCoO_3$. Therefore, three peaks are evident on deconvolution if the Co^{3+} states in Co_2O_3 and $LaCoO_3$ have different binding energy. The peaks of Co^{3+} state were found at binding energy 779.1eV and 780.1eV for Co_3O_4-$LaCoO_3$ [302, 303]. Both peaks got shifted by ≈ 1.1eV for Co/Co_3O_4-$LaCoO_3$ and Ni/ Co_3O_4-$LaCoO_3$, because of the interaction between active metals on impregnation. The difficulty in differentiating the Co^{3+} state was because it existed in both Co_3O_4 and $LaCoO_3$.

The comparative analysis of deconvoluted peaks of all catalysts has shown that on impregnation of Co_3O_4 the first peak intensity was increased, whereas intensity of second peak was comparable. Moreover, the first peak of Co^{3+} for Co_3O_4-$LaCoO_3$ and Ni/Co_3O_4-$LaCoO_3$ have relatively a low area as compared to the second. The area of Co^{2+} and first peak of Co^{3+} were contiguous to each other, which support the 1:1 atomic ratio of La and Co. Overall, this analysis concludes that the first and second peaks of Co^{3+} were for Co_3O_4 and $LaCoO_3$ respectively.

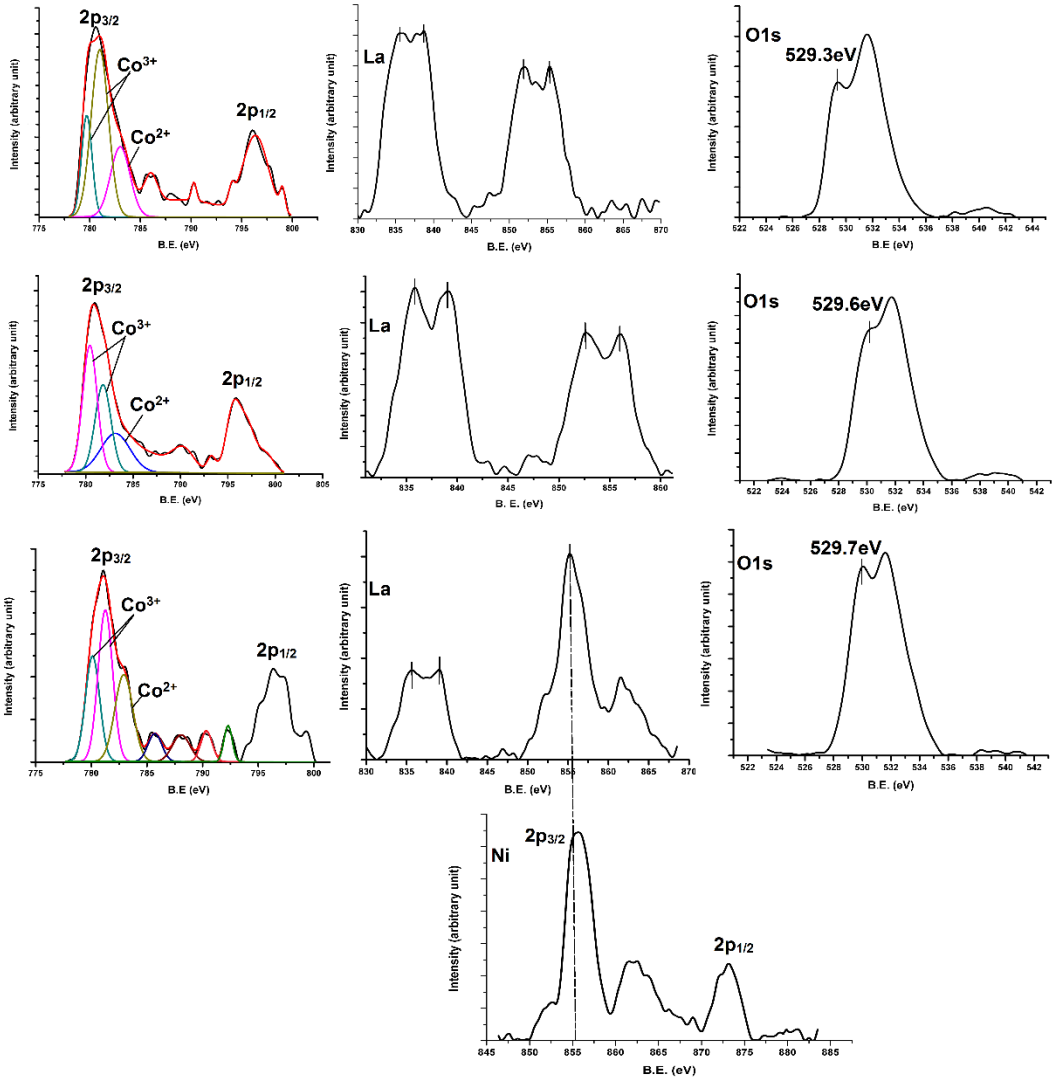

Figure 5.4 XPS profiles of Co_3O_4-$LaCoO_3$, Co/Co_3O_4-$LaCoO_3$ and Ni/ Co_3O_4-$LaCoO_3$

The XPS peak intensity of Ni was present in Figure 5.4 having binding energy ≈ 855eV. It is a common peak region for Ni$2p_{3/2}$ and the La$3d_{3/2}$.[302, 304] It is also evident from the comparative observation of XPS data for La each catalyst. The binding energy of La$3d_{5/2}$ region is about analogous for all catalysts, but La$3d_{3/2}$ region get altered only for Ni/Co_3O_4-$LaCoO_3$. The XPS peak intensity was relatively higher in the 855 eV region for Ni/ Co_3O_4-$LaCoO_3$ as compared to another catalysts. It favours the collective electron excitation of Ni $2p_{3/2}$ and La $3d_{3/2}$. Therefore, the Ni^{2+} state was confirmed by the $2p_{1/2}$ region of peak having binding energy ≈ 873.8 eV [305].

The oxygen can be present in three different forms, oxide, bridging and non-bridging in each catalyst. The binding energy of O1s in oxide form of every catalyst can be assigned at binding energy ≈ 529 eV. This peak intensity in this region becomes higher on impregnation with Co and Ni. It may be due to calcination of the catalyst after impregnation increases the overall oxygen in oxide form. The peaks having binding energy higher than 529 eV can be collective three peaks. The first two peaks for non-bridging of Co_3O_4 and $LaCoO_3$ (530.8 eV (for Co_3O_4), 531.6 eV) and one peak for bridging O at 534.3 eV [280, 306].

5.3.2. ESR performance test

The ethanol conversion was >90% for each catalyst above a temperature of 723K. But the product selectivity with desired gas (H_2) concentration was increased with increasing temperature. The optimum temperature was found 823K and 773K for Ni and Co loaded catalysts respectively. Nonetheless, the hydrogen selectivity of Ni/Co_3O_4-$LaCoO_3$ and Co/Co_3O_4-$LaCoO_3$ were 80% and 65% respectively. The comparative studies of product selectivity for the active metal loaded catalysts were analysed. The presence of double carbon containing compounds (C_2H_4 and CH_3CHO) in the produced gas indicate that the active metals have lower C-C bond scission at the particular temperature. The C_2H_4 formation was found to be more or less same at each temperature only for Co loaded catalyst, whereas Ni loaded catalyst checked C_2H_4 production completely above 773K. It indicates that Ni is more prominent in C-C bond scission relative to Co. It also concludes that Ni is highly active for C-C bond scission above 773K. The Ni presence has also diminished the CO formation from 673K-873K and 50% increment in the CO_2 selectivity. It can be considered due to water gas shift reaction (eq3.1).

The reaction mechanism involved during ESR can be analysed on the basis of product distribution of the gas mixture. The formation of C_2H_4, as well as CH_3CHO were found more prominent at low temperature. The product distribution for catalysts, Co/Co_3O_4-$LaCoO_3$ and Co_3O_4-$LaCoO_3$ reveals that further loading of Co did not affect the results considerably. It indicates that the used amount of Co for Co_3O_4-$LaCoO_3$ preparation was enough for the optimum activity of Co. Moreover, the activity of the cobalt persists after the proposed method of catalyst preparation. The effect of sintering of Co cannot be ignored, but their catalytic activity gets regenerated by the adopted method.

The increase in hydrogen selectivity ≈5% can be considered owing to interaction of Co_3O_4 with $LaCoO_3$. The addition of Ni as active metal facilitates the C-C bond scission of C_2H_4 and water gas shift reaction. The formed C_2H_4 due to dehydration of C_2H_5OH decomposes into carbon and hydrogen at a higher temperature (eq1.12). The carbon reacts with steam to form blue water gas (eq1.15). The Co as an active metal follows the path of ethanol dehydrogenation and decomposition of acetaldehyde into CH_4 and CO (eq1.8). It can also be observed from Figure 5.5 that the selectivity of CH_4 and CO were comparable.

Acetaldehyde formation up to 673K also favours this mechanism path during ESR. Decomposition of ethanol can also explain the similar selectivity of CH_4 and CO but the presence of acetaldehyde in product favours dehydrogenation mechanism. Moreover, the CO and CO_2 generation were abundant in case of Co/Co_3O_4-$LaCoO_3$ and Co_3O_4-$LaCoO_3$, but were lower for Ni/ Co_3O_4-$LaCoO_3$. It can be explained as methane steam reforming and water gas shift reaction (eq 1.22 and eq 3.1), which result in overall increase the H_2 selectivity[155].

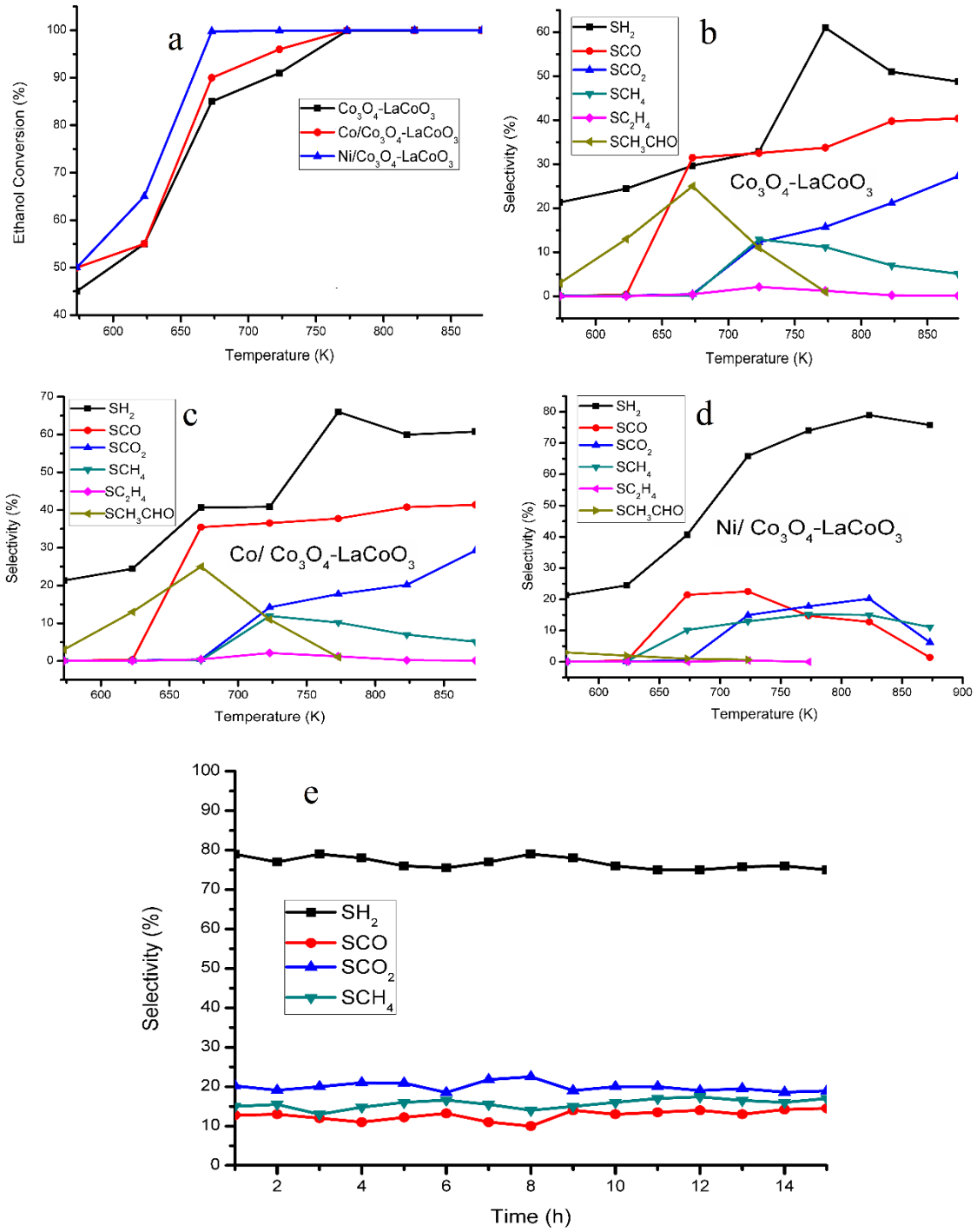

Figure 5.5 Catalytic activity graphs in terms of ethanol conversion (a) and product gas selectivity with temperature for Co_3O_4-$LaCoO_3$ (b), Co/Co_3O_4-$LaCoO_3$ (c), Ni/Co_3O_4-$LaCoO_3$ (d) each catalyst and TOS study for Ni/Co_3O_4-$LaCoO_3$.

The bimetallic interaction study of Ni and Cu with Al_2O_3 by Rogatis et al. has shown maximum hydrogen selectivity (≈80%) at temperature 873K, whereas in this work the similar selectivity of hydrogen was found with Ni/Co_3O_4-$LaCoO_3$ at a lower

temperature (823K) [298]. The bimetallic interaction of Ni and Co can be seen as a best catalytic performance by the experimental data obtained, and it is in agreement with the work of Zhao et al. [299]. It indicates that mixed oxides of Co and La act as better support as compared to Al_2O_3 and bimetallic effect of Co and Ni is better as compared to Ni and Cu. Zhao et al. [299] have reported the effect of B-site substitution in ABO_3 type perovskite with Ni and Co but the perovskite used as an active metal with ZrO_2 support [158]. The work suggests that the double carbon containing products (CH_3CHO and CH_3COCH_3) were generated at all temperatures (up to 1023K). Whereas, in this study the ESR with Ni/Co_3O_4-$LaCoO_3$, complete absence of double carbon-containing product (C_2H_4) after 773K was found. The selectivity of hydrogen was higher and comparable to that reported Zhao et al. [299] in the presence and absence of Ni respectively. It indicates that the cumulative effect of the bimetallic interaction of Ni and Co at B sites of perovskite structure is less significant as compared to impregnated surface bimetallic interaction for ESR. The time on stream study for ESR over Ni/Co_3O_4-$LaCoO_3$ at 873K has shown small decrease in 5% selectivity up to 15h (Figure 5.5).

5.4 Conclusion

The synthesized Co_3O_4-$LaCoO_3$ has significant activity with hydrogen generation (60%), but Co_3O_4-$LaCoO_3$ composite with Ni showed relatively higher selectivity (80%), especially at lower temperatures. The bimetallic Ni-Co interaction over Co_3O_4-$LaCoO_3$ composite as a support revealed substantial hydrogen selectivity.